

REYNOLDS NUMBER EFFECTS ON THE VORTEX STATE SWITCH OF UCAV MODEL

Yen-Po Chen, Jiun-Jih Miao, Yu-Hsin Chen*

Department of Aeronautics and Astronautics, National Cheng Kung University, Taiwan
*E-mail: asterr1228@gmail.com

Abstract

Reynolds number effects on the state switch of a vortex system on a lambda wing UCAV configuration were investigated using the techniques of flow visualization and pressure measurement. This wing model is characterized by spanwise-varying leading-edge contours. As a continuous effort of our previous studies, this work is focused on the behaviour of the inner vortex, which is an integral part of the vortex system developed above this UCAV model. Based on the results obtained, it is found that the inner vortex plays a key role in the state switch of the vortex system, which is sensitive to the angle of attack as well as Reynolds number. By flow visualization at Reynolds numbers of 10^3 to 10^4 , it is seen that the inner vortex is formed in the proximity of the junction of the main body and wing sections of the model at angles of attack 10° to 14° . By pressure measurements at Reynolds numbers of 10^5 and angles of attack 7° to 12° , a suction peak of pressure coefficient corresponding to the inner vortex structure is discerned. This suction peak gets diminished as Reynolds number increased.

Keyword: UCAV, lambda wing, flow visualization, oil-film, vortex system, inner vortex

1. Introduction

Aerodynamic research on UCAVs involves a comprehensive investigation into a wide range of Reynolds numbers. In this paper, an UCAV model named the UCAV NCKU model alike the SACCON model [1] was employed. It features a sharp-blunt-sharp leading-edge transformation from the wing apex to tip and with a 5-degree twist at the tip. As pointed out in the earlier studies [1-9], the vortical flow structures developed above the model are strongly dependent upon angle of attack named α hereafter.

A switch in flow topology state for α between 15° and 19° at Reynolds number 2.6×10^6 was noted by Schütte et al. [1] for the SACCON model. At $\alpha=15^\circ$, there are three vortical structures integrated as a vortex system dominating the flow field. Specifically, the apex vortex is referred to the one developed at sharp leading-edge, the thickness vortex is developed from the blunt leading-edge cross-sectional profile and the tip vortex is developed from the tip region of the wing. As α increased to 19° , the three vortices are merged into a primary vortex dominating the flow above the wing.

Experiments made at Reynolds numbers of 10^3 to 10^5 for the UCAV NCKU model unveil that the evolution of flow structures with α is involved in a complex process [2-5]. The states of the aerodynamic flow can be distinguished into three regimes with respect to α . Below $\alpha=10^\circ$, the attached flow is predominant above the wing surface. For $\alpha=10^\circ$ to $\alpha=15^\circ$, the vortex system comprising multiple vortices prevails over the model surface. Above $\alpha=17^\circ$, one primary vortex merged from the vortex system is predominant over the aerodynamic flow. Thus, the switch of the state regarding the aerodynamic flow is actually involved in a cascading process with α . Moreover, Chen [2] pointed out that an inner vortex was discerned at the junction between the main body and the wing sections of the model for $\alpha=10^\circ$ to 15° at Reynolds number of 10^4 to 10^5 , however it was not mentioned in Schütte et al. [1] for Reynolds number of 10^6 . Thus, effects of Reynolds number on the role of the inner vortex call for our attention.

In this study, experiments were carried out to study the characteristics of the inner vortex [2] above the UCAV NCKU model in a water channel and two wind tunnels, among which the Reynolds numbers could be ranged from 10^3 to 10^5 . The results obtained enable us to gain a better understanding on the role of the inner vortex involved in the aerodynamic flow around the wing model within the Reynolds number range studied, as well as make a comparison with the results reported in the literature, which were obtained at Reynolds numbers of one order higher. [1]

2. Methodology

2.1 Testing models

Four UCAV models of identical configuration but different sizes were employed in this study for flow visualization and pressure measurement. These models were made by a 3D printer and subsequently sandpapered and sprayed with water-proof paint. [2] It should be mentioned that while the model configuration was designed following the descriptions in Schütte et al. [1], no detailed dimensions of the models could be obtained from the open literature. Therefore, the present models made are named as the UCAV NCKU models.

Figure 1 shows the model for flow visualization with a root chord length $C_r = 170$ mm. Figure 2 depicts the model for pressure measurement whose $C_r = 400$ mm. There are 19 pressure taps indicated on the wing surface. In addition, a delta wing model of similar thickness distribution [2] to the UCAV NCKU model in Fig. 1 was employed in flow visualization experiment for comparison.

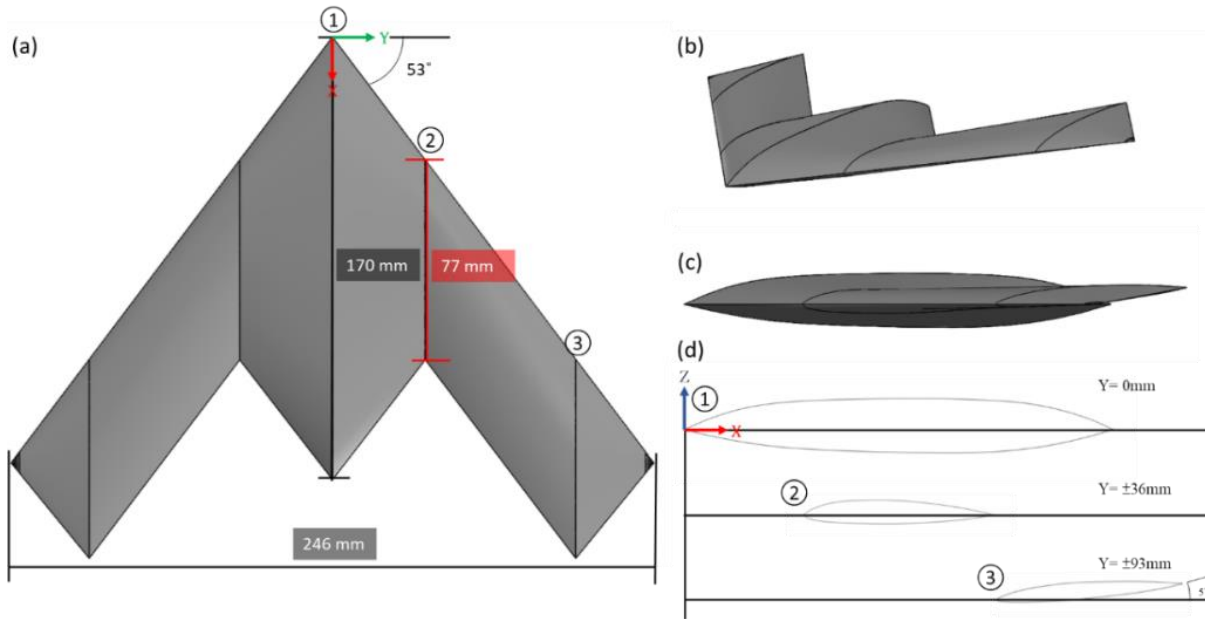


Fig. 1 Schematics of a UCAV NCKU model for flow visualization, (a) top view (b) overlook view (c) side view (d) cross-section.

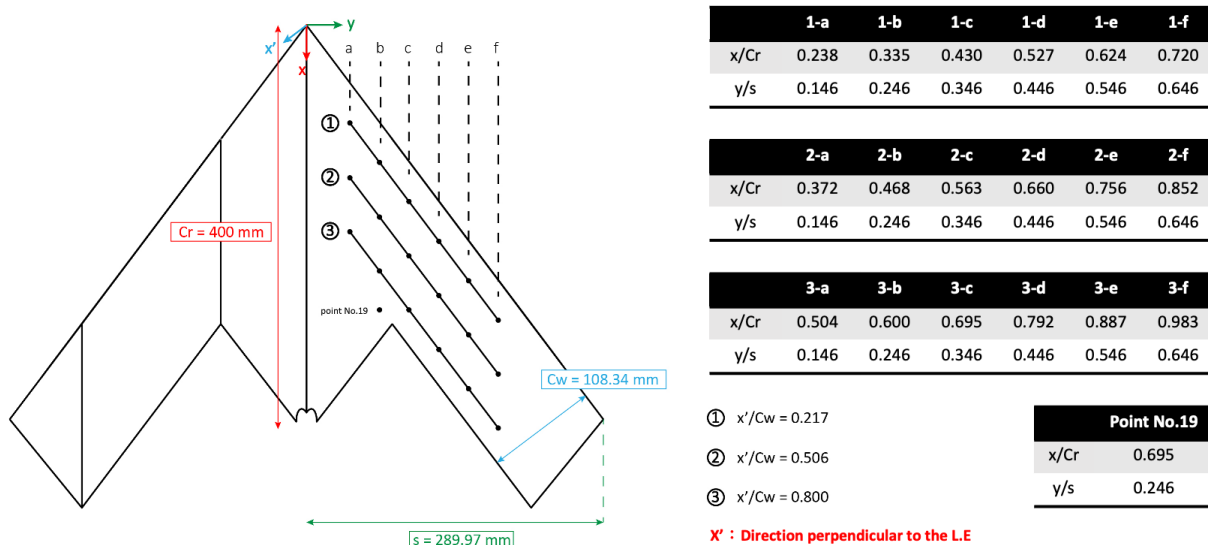


Fig. 2 Schematics of a UCAV NCKU model for pressure measurement and the coordinate system defined.

2.2 Experimental setup

Experiments were performed in three facilities, including a low-speed recirculating water channel with a square cross section 0.6 m by 0.6 m and 2.5 m in length [2], an open-jet low-speed wind tunnel with a 0.5 m

REYNOLDS NUMBER EFFECTS ON THE VORTEX STATE SWITCH OF UCAV MODEL

diameter circular test section and 2.5 m in length [3, 4], and an open loop wind tunnel with rectangular test section with 1 m in height and 1 m in width [5].

Experiments of dye-injection and ink-dot visualization were made in the water channel for the model described in Fig. 1 at $Re= 8.12 \times 10^3$, where Re denotes the Reynolds number based on the freestream velocity U and the chord length of the main body, Cr . Oil-flow visualization with the model in Fig. 1 and a Delta wing model [2] was conducted in the open-jet wind tunnel at $Re=1.01 \times 10^5$. Experiment with the pressure model described in Fig. 2 was conducted in the open-type wind tunnel at $Re= 1.20 \times 10^5$, 1.70×10^5 and 2.30×10^5 .

3. Results and Discussion

In this section, the flow visualization images are presented to enlighten the physical aspects of the aerodynamic flow, particularly on the inner vortex. The results of pressure measurements, in terms of the pressure coefficient C_p , are presented subsequently to further explain on the role of the inner vortex in the aerodynamic flow at α within a certain range, subjected to the experimental conditions studied.

3.1 Flow visualization in water channel for $Re= 8.12 \times 10^3$

Figure 3 presents two photo images obtained by the dye-injection and ink-dot visualization techniques, respectively, at $\alpha=10.1^\circ$, $Re= 8.12 \times 10^3$, a case of no formation of the inner vortex. In the left photo image, the red dye-streak released near the apex split into two branches as it approaching the junction between sharp and blunt leading-edge sections. To supplement the dye-streak appearance, the right photo image shows the limiting streamline pattern, which reveals that the spanwise motion of the flow from the apex affects a large portion of the wing area and converges to two locations marked by 1 and 2. Moreover, in the right photo image a flow reversal is indicated, which takes place from the trailing-edge of the main body section.

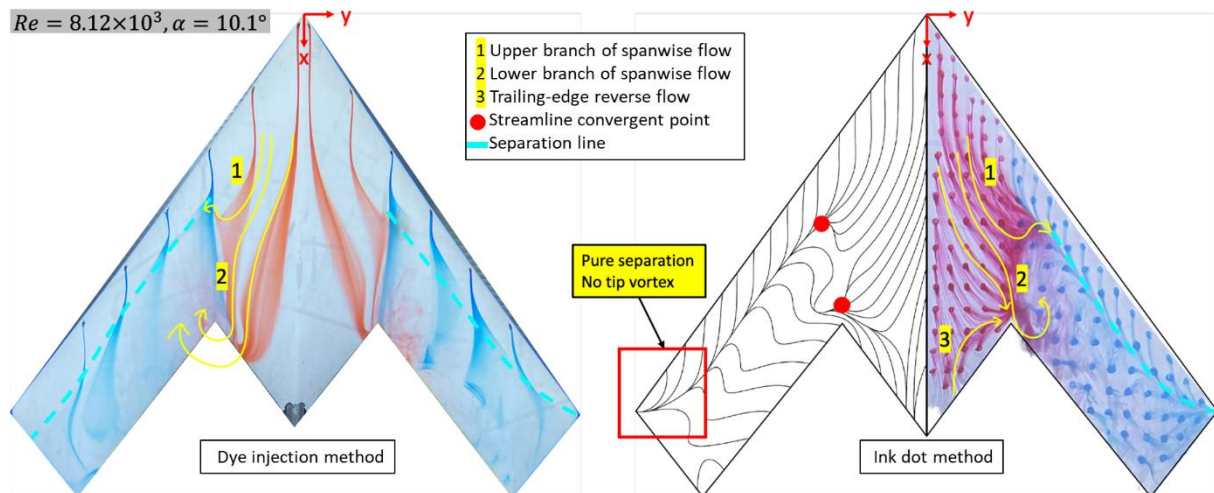


Fig. 3 Flow visualization images at $Re = 8.12 \times 10^3$, $\alpha = 10.1^\circ$. (left) Dye-injection. (right) Ink-dot.

Figure 4 shows the results of flow visualization at $\alpha=14.4^\circ$, a case that the inner vortex is clearly discerned. In detail, a weak vortex core is emerged from the dye streak originated from a point R4 at the leading edge of the main body section, an indication of the formation of apex vortex. At the same time, the dye streak originated from B2 at the leading edge of the blunt section unveils that the shear layer separated from at the leading-edge is entrained into a vortex, which is named the inner vortex [2]. By this vortical motion, the red streak from R4 and the blue streak from B2 are mixed into a single flow structure. Physically, the inner vortex is resulted by an interaction between the separated shear layer originated from the blunt leading-edge of the wing section and the spanwise flow as a component of the flow convecting from the apex. It is noteworthy that the inner vortex is not mentioned in the literature. [1, 7]

3.2 Flow visualization in wind tunnel at $Re= 7 \times 10^4$

In Fig. 5, the oil-film visualization image of the model obtained at $Re= 7 \times 10^4$ for $\alpha=10^\circ$ confirms the formation of the inner vortex on the present model. [2, 9] Essentially, the three-dimensional interaction of the spanwise cross-flow originated from the apex and the separated shear layer originated plays the key role in the formation of the inner vortex. An additional experiment made with a delta wing model (Fig. 5(b)) was purposely made to examine the effect due to the contoured geometry at the junction between the main body

and wing sections on the formation of the inner vortex. The result shows that the inner vortex forms regardless of the two planforms. Despite that there are the differences noted in the detailed features of the inner vortices of the two models, the general features of the two cases are rather alike. Thus, the contoured surfaces of both models lead to the formation of the inner vortex.

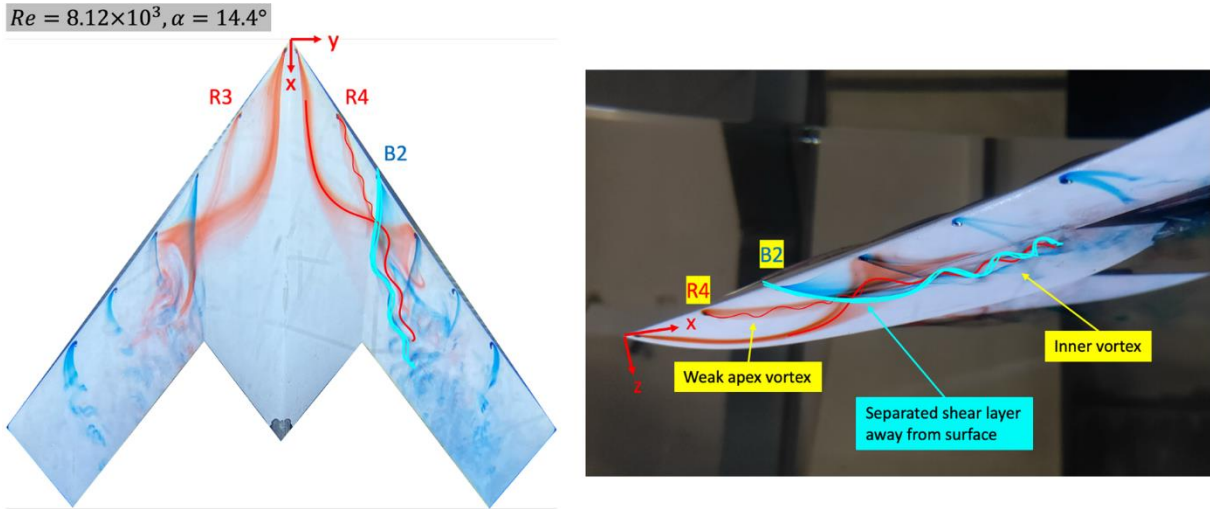


Fig. 4 Dye injection results under $Re = 8.12 \times 10^3$ at $\alpha = 14.4^\circ$. (left) Top view. (right) Side view.

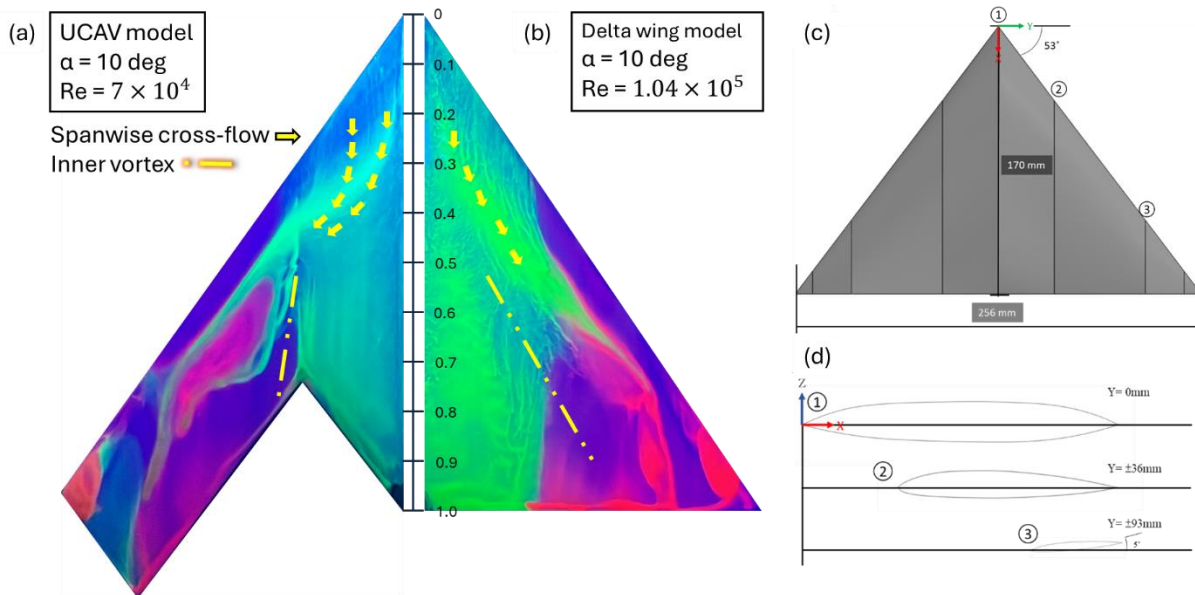


Fig. 5 Flow topology comparison between UCAV NCKU model the Delta-wing model.

3.3 Pressure measurement in wind tunnel for Re of 10^5

In this section, the results of pressure measurements obtained at $Re = 1.20 \times 10^5$, 1.70×10^5 and 2.30×10^5 are present for comparison and discussion.

Figure 6 shows variations of C_p at three taps aligned in the x direction at each of 6 spanwise locations measured, $y/s = 0.146$ to 0.646 , where y denotes the spanwise distance from the root chord and s denotes the length of the half span of the model, for $\alpha = 0^\circ$ to 20° , at $Re = 1.20 \times 10^5$. Notably, at pressure taps No.9 and 15, $y/s = 0.346$, the C_p values keep decreasing with α for $\alpha = 0^\circ$ to 5° . Subsequently, C_p at pressure tap No. 15 reaches a local minimum at $\alpha = 10^\circ$, whereas C_p at pressure tap No.9 keeps decreasing to higher α . The different trends of C_p at the two pressure taps around $\alpha = 10^\circ$ signifies that the formation of the inner vortex affects C_p at pressure tap No. 9. Similarly, the signature of the inner vortex can be found at pressure taps No. 10 and 11, which are located further outboard. At these pressure taps, the suction peak gets diminished as α increased beyond 10° . Moreover, a pronounced suction peak is noted for α within 15° and 20° depending on the pressure taps measured. The closer the pressure tap to the apex, the more significant the peak value. This is associated with the formation of the primary vortex. [2, 9] The data shown in the figure further suggest that the trajectory of the primary vortex core would be varied with α . However, it requires more data in order to

REYNOLDS NUMBER EFFECTS ON THE VORTEX STATE SWITCH OF UCAV MODEL

provide further description in this regard.

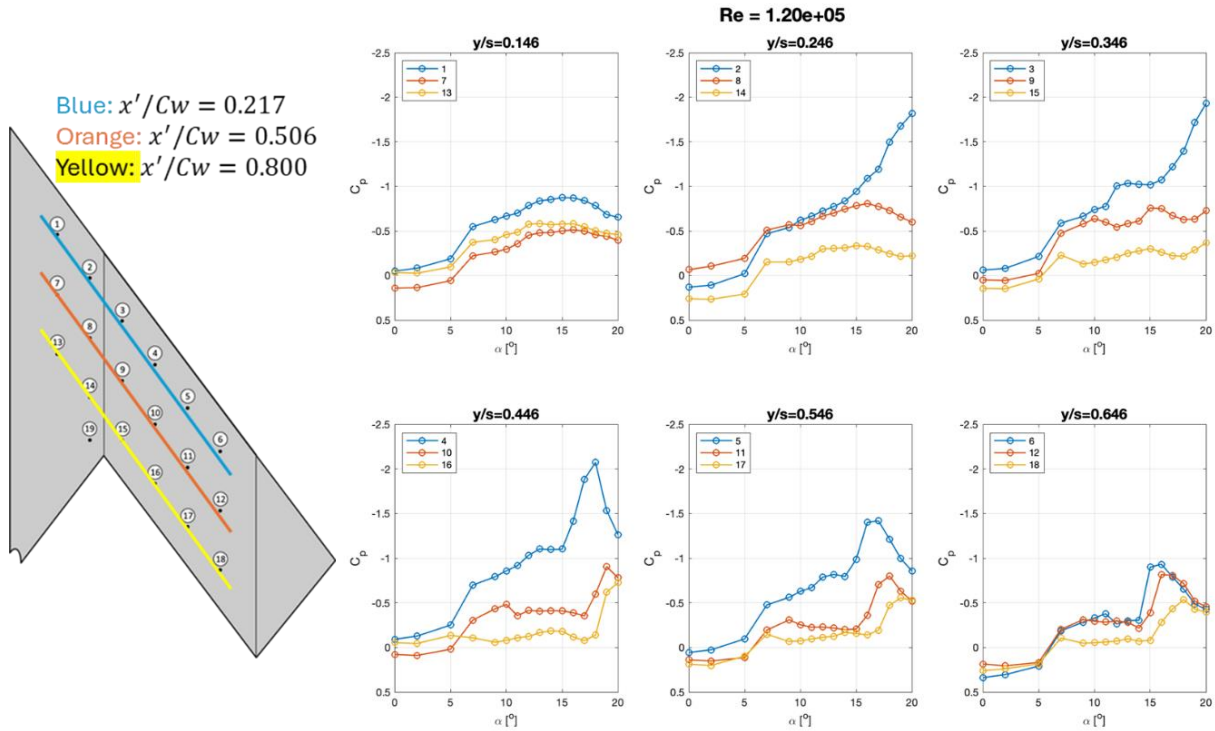


Fig. 6 C_p variations in the x direction at 6 spanwise positions on the model for $Re = 1.20 \times 10^5$.

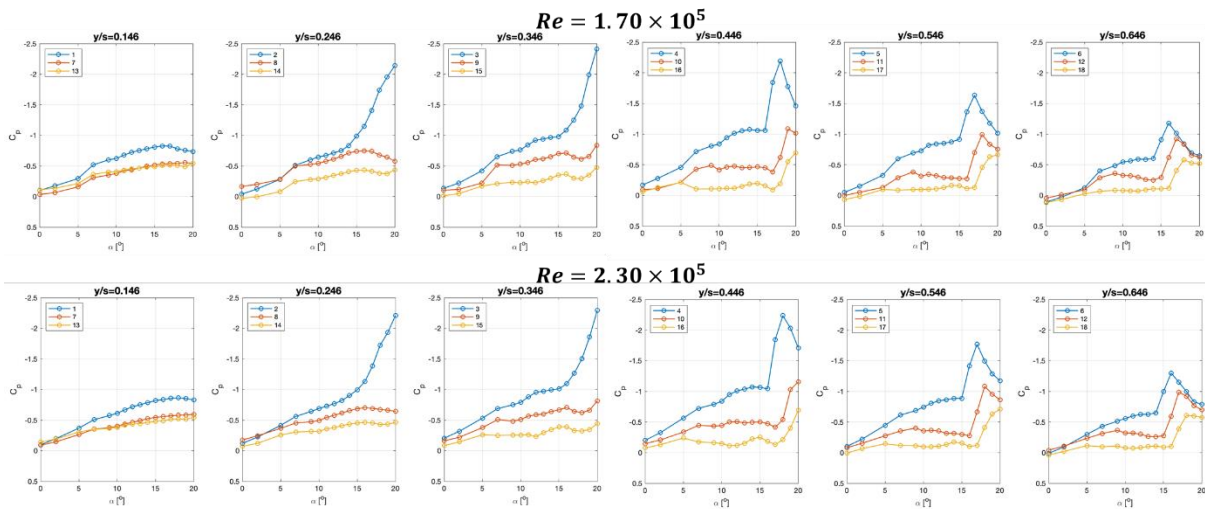


Fig. 7 C_p variations in the x direction at 6 spanwise positions on the model for $Re = 1.70 \times 10^5$ and 2.30×10^5

Figure 7 presents the results of pressure measurements obtained on the model at $Re=1.70 \times 10^5$ and 2.30×10^5 . Of particular concern, variations of C_p at pressure tap No.9 with Re are examined. At $Re=1.70 \times 10^5$, a suction peak of C_p is outstanding at α between 7° and 12° , inferring that the inner vortex is effective to the aerodynamic flow. However, at $Re=2.30 \times 10^5$, such a suction peak is almost diminished, therefore the effect of the inner vortex is rather not obvious. As concluded from the observations in Figs. 5 to 7 for the C_p variations at pressure tap No.9, it is clear that the inner vortex gets diminished at Re increased while Re is in the order of 10^5 . Supposedly, it would not be sensed at Re of 10^6 or higher. [1]

Physical explanation on the formation of the inner vortex for Re in the range of 10^3 to 10^5 is suggested as follows. As seen in flow visualization at 10^3 to 10^4 (Figs. 4 and 5), the spanwise motion of the fluid near the apex region plays a key role to the formation of the inner vortex. The spanwise motion near the surface essentially is driven by the thickness distribution of the wing in the apex region. For Re in the range of 10^3 to 10^5 , at low α , say 5° to 10° , flow in the region presumably is attached on the model surface as a three-dimensional, laminar boundary layer. Therefore, the downstream formation of the inner vortex is attributed to

the interaction with the separated shear layer originated from the blunt leading-edge of the wing section. However, at higher Re , for instance the case of $Re=2.30 \times 10^5$ in Fig. 7, at low α the boundary layer is speculated to get transition to turbulent, which results in higher momentum in the streamwise direction and reduce the momentum in the spanwise component, relatively speaking.

It is noteworthy that in the present study the switch of the state found around $\alpha=10^\circ$ is attributed to the formation of the inner vortex which gets diminished as Re increased beyond 10^5 . This is distinguishable from the finding in the literature [1] that a switch of the state took place on a SACCON model at $Re= 2.6 \times 10^6$, α between 15° and 19° , which is involved with the evolution of a vortex system of multiple vortices to a primary vortex. For the present model, such a switch of the state is also seen in the pressure measurement results at α between 15° and 20° .

4. Concluding remarks

This study reports on a switch of the vortex system state at Re of 10^3 to 10^5 at α about 10° , which is crucially dependent upon the formation of the inner vortex. The inner vortex produces a suction peak in the pressure distribution on the wing surface. In flow visualization, it is seen that the development of the inner vortex is due to the interaction of the three-dimensional boundary layer developed from the apex region and the separated shear flow originated from the blunt leading-edge of the wing section. As Re increased to 2.30×10^5 , the suction peak in the pressure distribution is suppressed. Thus, for the present model, the inner vortex only exists at Re of 10^5 or lower for α between 7° and 12° .

5. Acknowledgment

Funding support from National Science and Technology Council under the project number 112-2221-E-006-109 is gratefully acknowledged.

6. References

- [1] Schütte A., Hummel D., and Hitzel S.M., “Numerical and experimental analyses of the vortical flow around the SACCON configuration”, *Proc. 28th AIAA Applied Aerodynamics Conference*, Chicago, Illinois, 4690, (2010), pp. 2010-4690.
- [2] Chen Y.-H., “Vortex System Research on Spanwise-varying leading-edge contours of the UCAV configuration”, Master Thesis, Institute of Aeronautics and Astronautics, National Cheng Kung University, (2022).
- [3] Dong P., Miao J.-J., and Zoghalmi A., “An experimental study about drag crisis phenomenon on teardrop model”, *Journal of Aeronautics, Astronautics and Aviation*, Vol. 51, No. 2, (2019), pp 141-157.
- [4] Yu J., Leu T.-S., and Miao J.-J., “Investigation of reduced frequency and freestream turbulence effects on dynamic stall of a pitching airfoil”, *Journal of Visualization*, Vol. 20, (2017), pp 31-44.
- [5] Li, J.-Y., “Improvement on a Blade of a Vertical-Axis Wind Turbine”, Institute of Aeronautics and Astronautics, National Cheng Kung University, (2013).
- [6] Hummel D., “Effects of boundary layer formation on the vortical flow above slender delta wings”, *Proc. RTO AVT Specialists’ Meeting on “Enhancement of NATO Military Flight Vehicle Performance by Management of Interacting Boundary Layer Transition and Separation”*, Prague, Czech Republic, (2004), pp.30.
- [7] Zimper D. and Rein M., “Experimental and numerical analysis of the transonic vortical flow over a generic lambda wing configuration”, *Proc. 32nd AIAA Applied Aerodynamics Conference*, Atlanta, GA, 2005, (2014), pp 2014-2005.
- [8] Boelens O. J., Luckring J. M., Breitsamter C., Hövelmann A., Knoth F., Malloy D. J., and Deck S., “Numerical and theoretical considerations for the design of the AVT-183 diamond-wing experimental investigations”, *Proc. 53rd AIAA Aerospace Sciences Meeting*, Kissimmee, Florida, (2015), pp. 2015-0062
- [9] Chen Y.-H., Miao J.-J., Chen Y.-P., and Chen Y.-R., “Blunt leading-edge effect on spanwise-varying leading-edge contours of an UCAV configuration”, *Journal of Fluid Science and Technology*, Vol. 18, Issue 1, (2023), pp. JFST0012.